Commun. Comput. Phys.
doi: 10.4208/cicp.OA-2020-0184

Vol. **30**, No. 3, pp. 851-873
September 2021

A Hermite WENO Method with Modified Ghost Fluid Method for Compressible Two-Medium Flow Problems

Zhuang Zhao[1], Yong-Tao Zhang[2], Yibing Chen[3] and Jianxian Qiu[4,*]

[1] *School of Mathematical Sciences, Xiamen University, Xiamen, Fujian 361005, China.*
[2] *Department of Applied and Computational Mathematics and Statistics, University of Notre Dame, Notre Dame, IN 46556, USA.*
[3] *Institute of Applied Physics and Computational Mathematics, Beijing 100094, China.*
[4] *School of Mathematical Sciences and Fujian Provincial Key Laboratory of Mathematical Modeling and High-Performance Scientific Computing, Xiamen University, Xiamen, Fujian 361005, China.*

Received 19 September 2020; Accepted (in revised version) 1 February 2021

Abstract. In this paper, we develop a novel approach by combining a new robust finite difference Hermite weighted essentially non-oscillatory (HWENO) method [51] with the modified ghost fluid method (MGFM) [25] to simulate the compressible two-medium flow problems. The main idea is that we first use the technique of the MGFM to transform a two-medium flow problem to two single-medium cases by defining the ghost fluids status based on the predicted interface status. Then the efficient and robust HWENO finite difference method is applied for solving the single-medium flow cases. By using immediate neighbor information to deal with both the solution and its derivatives, the fifth order finite difference HWENO scheme adopted in this paper is more compact and has higher resolution than the classical fifth order finite difference WENO scheme of Jiang and Shu [14]. Furthermore, by combining the HWENO scheme with the MGFM to simulate the two-medium flow problems, less ghost point information is needed than that in using the classical WENO scheme in order to obtain the same numerical accuracy. Various one-dimensional and two-dimensional two-medium flow problems are solved to illustrate the good performances of the proposed method.

AMS subject classifications: 65M60, 35L65

Key words: Hermite WENO scheme, two-medium flow problems, modified ghost fluid method, Hermite interpolation.

*Corresponding author. *Email addresses:* zzhao@stu.xmu.edu.cn (Z. Zhao), yzhang10@nd.edu (Y.-T. Zhang), chen_yibing@iapcm.ac.cn (Y. Chen), jxqiu@xmu.edu.cn (J. Qiu)

1 Introduction

In this paper, a robust finite difference Hermite weighted essentially non-oscillatory (HWENO) method recently developed in [51] is combined with the modified ghost fluid method (MGFM) [25] to construct a novel approach in simulating the compressible two-medium flow problems. The compressible two-medium flow problems have different equation of state (EOS) across the material interface. This property causes challenge in designing efficient high order accuracy schemes since numerical oscillations or inaccuracies may easily appear in simulation results. In the literatures, there are two major ways to solve the compressible two-medium flow problems. One is the front capturing method, in which the high resolution methods with numerical diffusion or viscosity are used. The major advantages of the front capturing method are its ability to deal with large deformation problems and extension to high dimension easily, but the numerical inaccuracies or oscillations may still appear nearby the interface. Hence, there are various techniques introduced by e.g. Larrouturou [17], Karni [16], Abgrall et al. [1,2], Shyue et al. [39], Saurel et al. [36] and Chen et al. [7] to resolve this issue. The other one is the front tracking method, where the discontinuities between the two-medium flows are treated as internal moving interfaces. The method works very well across multi-material interfaces, however it could lead to the entanglement of the Lagrangian meshes, and the extension to high dimension is more difficult than the front capturing method. Classical works on the front tracking approach includes e.g. volume of fluid (VOF) method [12], level set method [40] and other front tracking methods [9,42].

To combine the advantages of the front capturing and tracking methods, Fedkiw et al. [8] constructed a new numerical method named as the ghost fluid method (GFM). In GFM, a level set function is used to track the interface in Eulerian schemes, which makes the interface "invisible". The pressure and velocity at the ghost fluid nodes near the material interface are defined as the local real values, while the density is obtained by isobaric fixing. The method transforms a two-medium flow problem to two single-medium flow problems via defining the ghost fluid status. Then, various state-of-the-art schemes for the single-medium flow problems can be applied straightforwardly. The GFM offers a flexible approach to solve the two-medium flow problems, furthermore, the extension of the method to solve high dimensional problems is fairly easy and straightforward. In complicated problems that a strong shock wave impacts on the interface, numerical inaccuracies often appear at the interface, if the wave interaction and material properties on both sides of the interface are not taken into account in the GFM. To solve this issue, Liu et al. [25] developed a modified ghost fluid method (MGFM), in which they defined the ghost fluid values using the predicted interfacial status obtained by solving a multi-material Riemann problem exactly or approximately. By taking the interaction of shock waves with the interface into account, the MGFM combines the advantages of the GFM [8] and the implicit characteristic methods [23,24]. Later on, the interface interaction ghost fluid method (IGFM) [13], the real ghost fluid method (RGFM) [43] and the practical ghost fluid method (PGFM) [44] were developed following the idea of the Riemann

problem-based methodology introduced in MGFM [25]. The MGFM is robust and less problem dependent, and it also has been applied in various problems in [19,22,28,32,46]. Its accuracy analysis and error estimation are performed in [21, 45]. While the GFM [8] and its relevant methods [13, 25, 43, 44] for solving two-medium flow problems are non-conservative near the interface, the conservative scheme is constructed in [31].

For solving the single-medium flow problems resulted from the MGFM, there are many successful numerical schemes. Among them, the class of high order accuracy finite difference or finite volume weighted essentially non-oscillatory (WENO) schemes is an excellent candidate. The first WENO scheme was designed by Liu, Osher and Chan [26] based on the ENO scheme [11], in which they developed a nonlinear convex combination of the approximations on all candidate stencils to achieve higher order accuracy in the smooth regions and eliminate non-physical oscillations in the discontinuous regions of numerical solutions simultaneously. Later, Jiang and Shu [14] constructed the third and fifth-order finite difference WENO schemes for high dimensional problems, where they gave a general framework for the definition of smoothness indicators and nonlinear weights. For more references of WENO, we refer to [3, 4, 20, 37]. In order to design a higher order WENO scheme, a wide stencil for the reconstructions have to be used. To obtain more compact schemes, Qiu and Shu [33, 34] developed a new finite volume scheme from WENO schemes via dealing with both the solution and its derivatives, named as Hermite WENO (HWENO) scheme. The HWENO schemes can achieve higher order numerical accuracy than the regular WENO schemes if the same spatial stencil is used. Motivated by this, HWENO schemes were further developed for hyperbolic conservation laws in [5, 27, 29, 41, 47, 52]. In these HWENO schemes, the derivatives or the first order moments of the solution were used directly, and different reconstruction polynomials were applied in the spatial discretization of the original equation and the equations satisfied by derivatives or the first order moments of the solution. It is quite difficult in this approach to maintain nonlinear stability and eliminate numerical oscillations near discontinuities of the solution. To resolve this issue, Zhao et al. [48, 50] modified the first order moments of the solution using HWENO procedure near the discontinuities, and the same polynomials to approximate the numerical fluxes of the original PDE and the derived equations were used. It was found that the HWENO modifications for the first order moments nearby the discontinuities lead to better performance in eliminating the nonlinear oscillations than the other HWENO schemes. Later, Zhao et al. [51] further extended this approach to the finite difference framework by modifying the derivatives of the solution to obtain a more robust and accurate scheme than the original one in [27]. Here we will use this robust modified finite difference HWENO method [51] to simulate the single-medium flow problems.

In this paper, we adopt the robust MGFM technique in [25] to predict the interfacial status by solving a multi-material Riemann problem exactly or approximately. The predicted interfacial values are then used to define the ghost fluid status and transform the two-medium flow problems to two single-medium flow problems. For the single-medium problems, we solve them by the newly developed modified finite difference

HWENO scheme [51]. The modified finite difference HWENO scheme [51] preserves the compact property of HWENO methods, i.e., only immediate neighbor information is used in the spatial reconstruction. This is a very good advantage to deal with the interface and boundary conditions in two-medium flow problems. For example, if the classical fifth order finite difference WENO scheme [14] with the MGFM is used, we have to define the ghost fluid status at 3 points, while only 2 ghost points are needed for the modified fifth order finite difference HWENO scheme [51] with the MGFM. Hence it is simpler to handle the material interface between two mediums. In summary, in this paper we will show that the modified fifth order finite difference HWENO scheme [51] combined with the MGFM [25] has the nice properties such as robustness, compactness and high resolution near discontinuities and is a suitable approach for simulating the two-medium flow problems.

The organization of the paper is as follows. In Section 2, we describe the detailed algorithm procedures of the modified fifth order finite difference HWENO scheme combined with the MGFM for solving two-medium flow problems. In Section 3, the numerical results for various gas-gas and gas-water interaction problems in one-dimension and two-dimension are presented to show the good performances of the proposed method. Concluding remarks are given in Section 4.

2 Numerical methods

In this section, we first present the governing equations for the one-dimensional and two-dimensional compressible two-medium flow problems, then briefly describe the modified finite difference HWENO method [51] for the single-medium case. Next, the level set technique is used to track the moving interface, and the modified ghost fluid method (MGFM) [25] is adopted to define the status of ghost fluids, by which the two-medium flow problems can be transformed to two single-medium cases. The single-medium cases are solved by the finite difference HWENO method [51]. At last, we give a summary of the overall implementation procedures.

2.1 Governing equations

The governing equations are the hyperbolic conservations laws

$$U_t+\nabla\cdot F(U)=0. \tag{2.1}$$

For one-dimensional Euler equations, U is $(\rho,\rho\mu,E)^T$ and $F(U)$ is $(\rho\mu,\rho\mu^2+p,\mu(E+p))^T$. For two-dimensional Euler equations, U is $(\rho,\rho\mu,\rho\nu,E)^T$, and $F(U)$ is $(F_1(U),F_2(U))$ with $F_1(U)=(\rho\mu,\rho\mu^2+p,\rho\mu\nu,\mu(E+p))^T$, $F_2(U)=(\rho\nu,\rho\mu\nu,\rho\nu^2+p,\nu(E+p))^T$, where ρ is the density, μ and ν are the velocity components in the x and y directions, respectively, p is the pressure, and E is the total energy. In addition, the equations of state (EOS) is needed

for the closure of the systems. Here, we use the γ-law for gas

$$\rho e = p/(\gamma-1),$$

and the EOS for the water medium [6, 8, 23]

$$\rho e = (p+N\bar{B})/(N-1),$$

where $\bar{B}=B-A$, $N=7.15$, $A=1.0\times10^5$ Pa, $B=3.31\times10^8$ Pa, and $\rho_0=1000.0kg/m^3$.

2.2 Finite difference HWENO scheme for single-medium case

The modified fifth order finite difference HWENO scheme [51] developed by Zhao et al. is more robust than the original finite difference HWENO scheme [27], and has the advantages that no additional positivity-preserving flux limiter methodology is required and a larger CFL number can be used. It also has a higher order numerical accuracy than the original finite difference HWENO scheme [27] for two-dimensional problems. The modified HWENO scheme is more compact than the classical fifth order finite difference WENO scheme [14] since only immediate neighbor information is needed in the reconstruction, which makes the HWENO scheme have smaller numerical errors and higher resolutions. Due to these good properties of the modified HWENO scheme [51], we choose this method to solve the single-medium flow problems. To the authors' knowledge, this is the first time that the HWENO method is used in the simulations of the compressible two-medium flow problems. To save space, here we briefly review the essential procedure of the modified HWENO scheme in [51].

For the one-dimensional case, we first consider the following scalar equation

$$\begin{cases} u_t+f_x(u)=0, \\ u(x,0)=u_0(x). \end{cases} \tag{2.2}$$

In the finite difference framework, the computation domain is divide by uniform grid points $\{x_i\}$, and $x_{i+1/2}$ is defined as $x_i+\Delta x/2$, where Δx is the grid size $x_{i+1}-x_i$. I_i denotes the cell $[x_{i-1/2},x_{i+1/2}]$. To design a Hermite WENO scheme, we take partial derivative w.r.t the variable x on the governing equation (2.2) and denote the partial derivative of $u(x,t)$ w.r.t x by a new function $v(x,t)$. Then we have

$$\begin{cases} u_t+f(u)_x=0, \quad u(x,0)=u_0(x), \\ v_t+h(u,v)_x=0, \quad v(x,0)=v_0(x), \end{cases} \tag{2.3}$$

where $h(u,v)=f(u)_x=f'(u)u_x=f'(u)v$, and $v(x,0)=u_x(x,0)$. The semi-discrete finite difference scheme for solving (2.3) is

$$\begin{cases} \dfrac{du_i(t)}{dt}=-\dfrac{1}{\Delta x}\left(\hat{f}_{i+1/2}-\hat{f}_{i-1/2}\right), \\ \dfrac{dv_i(t)}{dt}=-\dfrac{1}{\Delta x}\left(\hat{h}_{i+1/2}-\hat{h}_{i-1/2}\right), \end{cases} \tag{2.4}$$

where the numerical fluxes $\hat{f}_{i+1/2}$ and $\hat{h}_{i+1/2}$ are the fifth order approximation of $\Phi_{i+1/2}=\Phi(x_{i+1/2})$ and $\Psi_{i+1/2}=\Psi(x_{i+1/2})$, respectively. $\Phi(x)$ and $\Psi(x)$ are defined implicitly as

$$f(u(x))=\frac{1}{\Delta x}\int_{x-\Delta x/2}^{x+\Delta x/2}\Phi(x)dx,\quad h(u(x),v(x))=\frac{1}{\Delta x}\int_{x-\Delta x/2}^{x+\Delta x/2}\Psi(x)dx.$$

For the purpose of upwinding, we split the flux $f(u)$ and $h(u,v)$ into two parts: $f(u)=f^+(u)+f^-(u)$ and $h(u,v)=h^+(u,v)+h^-(u,v)$, in which $\frac{df^+(u)}{du}\geq 0$, $\frac{\partial h^+(u,v)}{\partial v}\geq 0$ and $\frac{df^-(u)}{du}\leq 0$, $\frac{\partial h^-(u,v)}{\partial v}\leq 0$, respectively. Here, we apply the global Lax-Friedrichs flux splitting

$$f^{\pm}(u)=\frac{1}{2}(f(u)\pm\alpha u)\quad\text{and}\quad h^{\pm}(u,v)=\frac{1}{2}(h(u,v)\pm\alpha v),$$

where $\alpha=\max_u|f'(u)|$. The reconstructions of $\hat{f}^{\pm}_{i+1/2}$ and $\hat{h}^{\pm}_{i+1/2}$ are for the fluxes $f^{\pm}(u)$ and $h^{\pm}(u,v)$, respectively. The final numerical fluxes $\hat{f}_{i+1/2}=\hat{f}^{+}_{i+1/2}+\hat{f}^{-}_{i+1/2}$ and $\hat{h}_{i+1/2}=\hat{h}^{+}_{i+1/2}+\hat{h}^{-}_{i+1/2}$. Next, we present the reconstruction procedure for the numerical fluxes $\hat{f}^{\pm}_{i+1/2}$ and $\hat{h}^{\pm}_{i+1/2}$, and it is consisted of the following two steps.

Step 1. Modify the derivative of the solution.

Since the solution of non-linear hyperbolic conservation laws often contains discontinuities where the derivative of the solution is very large, this may lead to the non-physical oscillations of numerical solution in the discontinuous regions if high order HWENO schemes are not designed carefully. In the modified HWENO scheme [51], we modify the derivative value v_i as described in the following. It makes this new HWENO scheme more robust than its previous versions.

Firstly, using three small stencils $S_1=\{x_{i-1},x_i\}$, $S_2=\{x_{i-1},x_i,x_{i+1}\}$ and $S_3=\{x_i,x_{i+1}\}$, we construct three quadratic polynomials $p_1(x),p_2(x),p_3(x)$ on S_1,S_2,S_3 by Hermite interpolation respectively, which satisfy

$$\begin{aligned}
&p_1(x_{i+l})=u_{i+l},\ l=-1,0,\quad p_1'(x_{i-1})=v_{i-1},\\
&p_2(x_{i+l})=u_{i+l},\ l=-1,0,1,\\
&p_3(x_{i+l})=u_{i+l},\ l=0,1,\quad p_3'(x_{i+1})=v_{i+1}.
\end{aligned}$$

Then, we use their derivative values $p_n'(x_i)$ $(n=1,2,3)$ to modify the derivative value v_i as the following

$$v_i^{new}=\sum_{n=1}^{3}\omega_n p_n'(x_i),$$

where v_i^{new} is the modified value of v at the point x_i and ω_n is the non-linear weight, and the nonlinear convex combination of $p_n'(x_i)(n=1,2,3)$ provides the fifth order accuracy for the modification of v_i in the smooth regions. The specific formulas including the non-linear weight ω_n and the polynomial derivative value $p_n'(x_i)$ can be found in [51].

Step 2. Reconstruct the numerical fluxes $\hat{f}^{\pm}_{i+1/2}$ and $\hat{h}^{\pm}_{i+1/2}$.

We only describe the reconstruction procedures for $\hat{f}^{+}_{i+1/2}$ and $\hat{h}^{+}_{i+1/2}$, while the reconstruction procedures of the negative wind numerical fluxes $\hat{f}^{-}_{i+1/2}$ and $\hat{h}^{-}_{i+1/2}$ are similar. Firstly, the same stencils S_1,S_2,S_3 in Step 1 are used to reconstruct three cubic polynomials $p_1(x),p_2(x),p_3(x)$ on S_1,S_2,S_3, which satisfy

$$\begin{aligned}
&\frac{1}{\Delta x}\int_{I_{i+l}} p_1(x)dx = f^+(u_{i+l}),\ l=-1,0, \quad \frac{1}{\Delta x}\int_{I_{i-1}} p_1'(x)dx = h^+(u_{i-1},v_{i-1}),\\
&\frac{1}{\Delta x}\int_{I_i} p_1'(x)dx = h^+(u_i,v_i^{new}),\\
&\frac{1}{\Delta x}\int_{I_{i+l}} p_2(x)dx = f^+(u_{i+l}),\ l=-1,0,1, \quad \frac{1}{\Delta x}\int_{I_i} p_2'(x)dx = h^+(u_i,v_i^{new}),\\
&\frac{1}{\Delta x}\int_{I_{i+l}} p_3(x)dx = f^+(u_{i+l}),\ l=0,1, \quad \frac{1}{\Delta x}\int_{I_{i+1}} p_3'(x)dx = h^+(u_{i+1},v_{i+1}),\\
&\frac{1}{\Delta x}\int_{I_i} p_3'(x)dx = h^+(u_i,v_i^{new}).
\end{aligned}$$

Then, $\hat{f}^{+}_{i+1/2}$ is computed based on the function values $p_n(x_{i+1/2})$, $n=1,2,3$ as follows,

$$\hat{f}^{+}_{i+1/2} = \sum_{n=1}^{3} \omega_n^f p_n(x_{i+1/2}),$$

where ω_n^f is the non-linear weight associated with the reconstruction for $\hat{f}^{+}_{i+1/2}$. The derivative values $p_n'(x_{i+1/2})$, $n=1,2,3$ are used to reconstruct $\hat{h}^{+}_{i+1/2}$:

$$\hat{h}^{+}_{i+1/2} = \sum_{n=1}^{3} \omega_n^h p_n'(x_{i+1/2}),$$

where ω_n^h is the non-linear weight associated with the reconstruction for $\hat{h}^{+}_{i+1/2}$. Again, the detailed formulas for the non-linear weights ω_n^f and ω_n^h, the polynomial value $p_n(x_{i+1/2})$ and its derivative value $p_n'(x_{i+1/2})$ can be found in [51].

After the spatial discretization, the semi-discrete scheme (2.4) is solved by the third order TVD Runge-Kutta method [38] as follows,

$$\begin{cases}
U^{(1)} = U^n + \Delta t L(U^n),\\
U^{(2)} = \frac{3}{4}U^n + \frac{1}{4}U^{(1)} + \frac{1}{4}\Delta t L(U^{(1)}),\\
U^{(n+1)} = \frac{1}{3}U^n + \frac{2}{3}U^{(2)} + \frac{2}{3}\Delta t L(U^{(2)}),
\end{cases} \tag{2.5}$$

where $U=(u,v^{new})^T$ for the one-dimensional case.

For the two-dimensional case, we first consider the scalar equation

$$\begin{cases} u_t+f(u)_x+g(u)_y=0, \\ u(x,y,0)=u_0(x,y). \end{cases} \tag{2.6}$$

Similarly, the spatial domain is partitioned by a uniform mesh with grid points $\{(x_i,y_j)\}$. The grid sizes $\Delta x=x_{i+1}-x_i$ and $\Delta y=y_{j+1}-y_j$, and the half grid points $x_{i+1/2}=x_i+\Delta x/2$ and $y_{j+1/2}=y_j+\Delta y/2$. The cell $I_{i,j}$ is defined as $[x_{i-1/2},x_{i+1/2}]\times[y_{j-1/2},y_{j+1/2}]$, and its center is (x_i,y_j). In order to design a HWENO scheme, we take the partial derivatives on both sides of the governing equation (2.6) with respect to the x and y variables, respectively, and introduce two new variables $v=u_x$ and $w=u_y$. Then the following equations are obtained:

$$\begin{cases} u_t+f(u)_x+g(u)_y=0, & u(x,y,0)=u_0(x,y), \\ v_t+h(u,v)_x+r(u,v)_y=0, & v(x,y,0)=v_0(x,y), \\ w_t+q(u,w)_x+s(u,w)_y=0, & w(x,y,0)=w_0(x,y), \end{cases} \tag{2.7}$$

where

$$\begin{aligned} &h(u,v)=f'(u)v, \quad r(u,v)=g'(u)v, \quad v(x,y,0)=u_x(x,y,0); \\ &q(u,w)=f'(u)w, \quad s(u,w)=g'(u)w, \quad w(x,y,0)=u_y(x,y,0). \end{aligned}$$

Notice that Eqs. (2.3) and (2.7) have some common points. For example, $f(u)_x$ and $g(u)_y$ are associated with $h(u,v)_x$ and $s(u,w)_y$, respectively. The spatial discretizations in solving the one-dimensional case can be directly extended here for these four terms. The discretizations for the mixed derivative terms $q(u,w)_x$ and $r(u,v)_y$ are not in the one-dimensional case, and they are discussed in the next. Then we obtain the semi-discrete finite difference scheme of (2.7) as follows,

$$\begin{cases} \dfrac{du_{i,j}(t)}{dt}=-\dfrac{1}{\Delta x}\left(\hat{f}_{i+1/2,j}-\hat{f}_{i-1/2,j}\right)-\dfrac{1}{\Delta y}\left(\hat{g}_{i,j+1/2}-\hat{g}_{i,j-1/2}\right), \\ \dfrac{dv_{i,j}(t)}{dt}=-\dfrac{1}{\Delta x}\left(\hat{h}_{i+1/2,j}-\hat{h}_{i-1/2,j}\right)-\dfrac{1}{\Delta y}\left(\hat{r}_{i,j+1/2}-\hat{r}_{i,j-1/2}\right), \\ \dfrac{dw_{i,j}(t)}{dt}=-\dfrac{1}{\Delta x}\left(\hat{q}_{i+1/2,j}-\hat{q}_{i-1/2,j}\right)-\dfrac{1}{\Delta y}\left(\hat{s}_{i,j+1/2}-\hat{s}_{i,j-1/2}\right). \end{cases} \tag{2.8}$$

The next step is to reconstruct the numerical fluxes $\hat{f}_{i\pm1/2,j}$, $\hat{h}_{i\pm1/2,j}$, $\hat{g}_{i,j\pm1/2}$, $\hat{s}_{i,j\pm1/2}$, $\hat{q}_{i\pm1/2,j}$ and $\hat{r}_{i,j\pm1/2}$.

Just as one-dimensional case, the reconstruction procedure is consisted of the following two steps. The first step is to modify the partial derivative of the solutions on all grid points in the dimension-by-dimension way. The second step is to reconstruct these six numerical fluxes. The numerical fluxes $\hat{f}_{i\pm1/2,j}$, $\hat{h}_{i\pm1/2,j}$, $\hat{g}_{i,j\pm1/2}$ and $\hat{s}_{i,j\pm1/2}$ are reconstructed in the dimension-by-dimensional manner, while the mixed derivative terms $\hat{q}_{i\pm1/2,j}$ and $\hat{r}_{i,j\pm1/2}$ are reconstructed by a linear approximation since we have used HWENO technique to modify the partial derivatives $v_{i,j}$ and $w_{i,j}$ for all points in the first step. The details for the first and second steps can be found in [51].

After the spatial discretization, the semi-discrete scheme (2.8) is evolved in time by the third order TVD Runge-Kutta method, and the formulas are given in (2.5) with $U=(u,v^{new},w^{new})^T$ for two-dimensional case.

Remark 2.1. For the system case, such as one-dimensional and two-dimensional compressible Euler equations, all HWENO procedures are performed on the local characteristic field as in [14], while the linear approximation in the procedure for two-dimensional case is applied in the component-wise.

2.3 Level set equation

The material interface moves with the velocity of the fluids between two mediums, which is tracked by the level set method in this paper. For one-dimensional case, the moving interface is modeled by the level set equation as follows

$$\phi_t+\mu\phi_x=0, \tag{2.9}$$

and for two-dimensional case, it is

$$\phi_t+\mu\phi_x+\nu\phi_y=0, \tag{2.10}$$

where ϕ is a signed distance function. μ and ν are the velocity of the fluids in the x and y directions, respectively. The level set equations (2.9) and (2.10) are two Hamilton-Jacobi equations, which are solved by the hybrid fifth order finite difference WENO method introduced in [49] (see the Appendix A there). The level set method may cause seriously distorted contours in the case that the velocity field has a large gradient near the interface. Here, we re-distribute the signed distance function ϕ to remedy this issue, which is the re-initialization technique. For one-dimensional case, the exact location of the interface can be obtained by Newton's iteration method, then, we re-distribute the signed distance function ϕ based on its definition. For two-dimensional problems, the material interface between two mediums is a curve, so it is difficult to use the re-distribution technique in one-dimensional case. Instead we solve the following re-initialization equation

$$\phi_t+S(\phi_0)\big(\sqrt{\phi_x^2+\phi_y^2}-1\big)=0, \tag{2.11}$$

where S is the sign function of ϕ_0. The re-initialization equation (2.11) is also a Hamilton-Jacobi equation, and it is solved by the hybrid WENO method in [49] (see the Appendix A there). Other methods for solving Hamilton-Jacobi equations can be applied too, e.g., a recently developed arbitrary Lagrangian-Eulerian finite difference WENO scheme for Hamilton-Jacobi equations in [18].

2.4 Modified ghost fluid method

The modified ghost fluid method (MGFM) developed by Liu et al. [25] is mainly based on the GFM [8], but the MGFM uses the predicted interfacial status to define the ghost

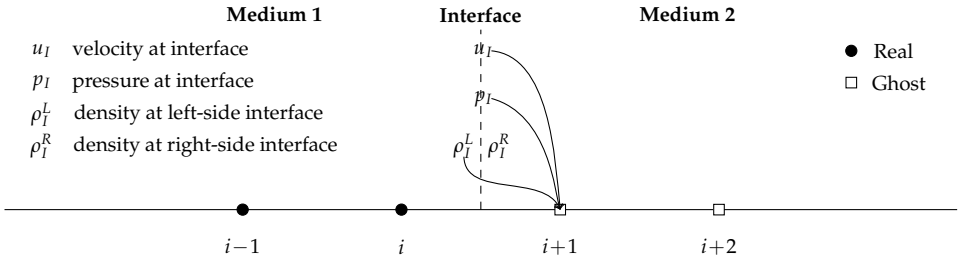

Figure 1: Isentropic fixing for 1D two-medium flow problems.

fluid values, which takes the interaction of shock with the interface into consideration, therefore, the MGFM is more robust and less problem related. Considering the good performances of the MGFM, we would apply it to define the ghost fluid values, then, it turns a two-medium flow problem into two single-medium flow problems, and we would review the MGFM in the next procedures for one-dimensional and two-dimensional cases. The main procedures are that we first predict the interface status by solving a two-medium Riemann problem exactly or approximately, then, the predicted interface status is used to define the ghost fluid status for each medium.

For one-dimensional case, we only take the definition of the ghost fluid status for Medium 1 as an example, while the procedure for Medium 2 is similar. Suppose that the interface is located between the points i and $i+1$ in Fig. 1, then, the statuses of U_{i-1} and U_{i+2} are applied to define the two-medium Riemann problem suggested in [25], and we can obtain the interfacial status by solving the two-medium Riemann problem exactly or approximately as u_I (velocity), p_I (pressure), ρ_I^L (density at left-side) and ρ_I^R (density at right-side), then, the velocity, pressure and density at the ghost point $i+1$ are directly defined as the predicted values u_I, p_I, ρ_I^L, while for the points i and $i+2$, the pressure and velocity are the real values on the local fluid, but the density at the two points is replaced by the isentropic fixing [8,25], and the derivative values at these points are set as zero at the same time. Certainly, the classical fifth order WENO scheme [14] combined with the modified ghost fluid method (MGFM) [25] needs to add the definition of the fluid status at points $i-2$ and $i+3$ for two mediums.

For two-dimensional case, there is two velocity components, which means the two-medium Riemann problem can't be simply defined as one-dimensional case. Fortunately, we have known the normal direction $\overrightarrow{n}$ near the interface based on the level set function ($\overrightarrow{n}=\nabla\phi/|\nabla\phi|$), then, we can define the two-medium Riemann problem following the normal direction. More explicitly, we calculate the normal velocity u_N and tangential velocity u_T near the interface, where u_N is defined as $(\mu,\nu)\cdot\overrightarrow{n}$. Next, the normal velocity u_N, the pressure p and the density ρ are used to define the two-medium Riemann problem as one-dimensional case. In terms of the MGFM [25] and the modified HWENO scheme [51], we only need to define the fluid status of the computational domain for each medium including boundary and grid points in the interfacial regions by $|\phi|<2\max(\Delta x,\Delta y)$, and the size of the band is decided by the scheme for solving the

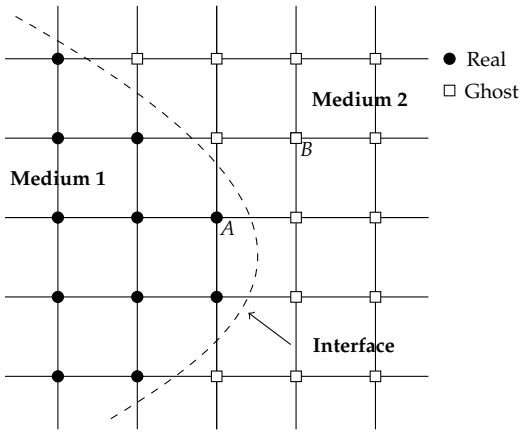

Figure 2: Isentropic fixing for 2D two-medium flow problems.

single-medium flow problems, while the classical fifth order WENO scheme [14] needs to define the fluid status of the computational domain with $|\phi| < 3\max(\Delta x, \Delta y)$. Later, we take the definition of the status for Medium 1 at the points A (seen in Fig. 2) as an example, while the definition of the information for Medium 2 is similar. First of all, we need to find other point next to the interface ($|\phi| < 2\max(\Delta x, \Delta y)$) located in the Medium 2, and the angle made by the normal of the two points must be the minimum. Suppose that the point B meets the requirements, then, the two-medium Riemann problem in the normal direction is defined as

$$U|_{t=t_n} = \begin{cases} U_A, \\ U_B, \end{cases}$$

where $U_A = (\rho^A, u_N^A, p^A)$ and $U_B = (\rho^B, u_N^B, p^B)$, which can be solved approximately or exactly, then, we obtain the predicted status u_I (velocity), p_I (pressure), ρ_I^A (density at A-side) and ρ_I^R (density at B-side). Similarly as one-dimensional case, we only need to define the density at node A by isentropic fixing [8, 25], while the statuses at node B are defined by u_I, p_I and ρ_I^A, and their tangential velocity is still the original value. At the same time, the derivative values at nodes A and B are set as zero too.

Remark 2.2. The GFM and its relevant methods including MGFM [25], IGFM [13], RGFM [43] and PGFM [44] for solving compressible two-medium flow problems are all non-conservative near the interface. A conservative scheme is designed in [31], which is mainly based on the discontinuous Galerkin framework. We will use this idea to design a conservative HWENO scheme in the future work.

2.5 Summary of the procedures

At the end of this section, we briefly summarize the whole procedures for the simulation of two-medium flow problems. Suppose the solution for the governing equations at time t_n has been obtained, then we advance the solution to time t_{n+1} as the following:

Step 1. Compute the time step Δt_n, which satisfies the stability condition over the whole range.

Step 2. Calculate the level set equation, and obtain the new location of the interface at the next intermediate time step shown in Section 2.3.

Step 3. Define and solve the two-medium Riemann problem nearby the interface to obtain the predicted interface status, and define the ghost fluid values for Mediums 1 and 2, respectively, introduced in Section 2.4.

Step 4. Solve the governing equations by the modified HWENO method to the next intermediate time step given in Section 2.2 for Mediums 1 and 2, respectively.

Step 5. Repeat Step 2 to Step 4 for each sub-step of the third order Runge-Kutta temporal discretization method, advancing the solution from U_n to U_{n+1}, then, re-initialize the level set function.

Remark 2.3. The MGFM transforms a two-medium flow problem to two single-medium flow problems, and we use the HWENO method to solve them. It costs the HWENO scheme slightly more computational time than that of WENO schemes on the same meshes, but the HWENO scheme is much more compact as only immediate neighbor information is used in the reconstructions, which makes the HWENO scheme have less numerical errors and higher resolution. This is observed in [51] for the single-medium flow problems. Furthermore, the HWENO scheme is easier to implement on the modern parallel machines and unstructured meshes as it only uses the information on the target cell and its immediate neighbor cells, while the fifth order WENO scheme [14] needs to add the next layer neighbor information of the immediate neighbor cells. In addition, the MGFM needs to define the information on the ghost points by solving a two-medium Riemann problem near the interface, and it is difficult for accurate definition of values on multiple layers of ghost points.

3 Numerical results

In this section, we present the numerical results of the modified fifth order finite difference HWENO scheme [51], classical fifth order finite difference WENO scheme [14] and improved fifth order finite difference WENO-Z scheme [4] with the modified ghost fluid method [25] for two-medium flow problems which are introduced in the previous section. And we can see three schemes have similar results, but the HWENO scheme is more compact than the WENO scheme as only immediate neighbor information is used in the reconstructions. The CFL number is 0.6. The units for the density, velocity, pressure, length and time are kg/m^3, m/s, Pa, m, and s, respectively.

Example 3.1. This problem contains two different gases taken from [8]. The initial conditions are

$$(\rho,\mu,p,\gamma)=\begin{cases}(1,0,1\times10^5,1.4), & x\in[0,0.5),\\ (0.125,0,1\times10^4,1.2), & x\in[0.5,1],\end{cases}$$

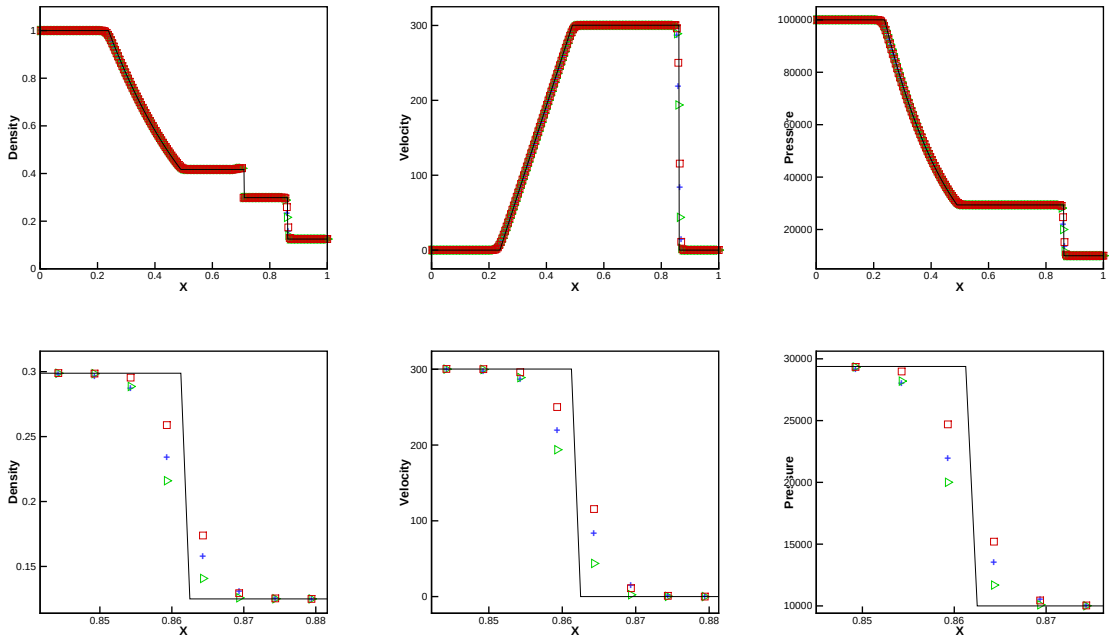

Figure 3: Example 3.1. $t=0.0007$. From left to right: density; velocity; pressure. From top to bottom: the computed results and their partial enlarged view. Solid line: the exact solution; plus signs: the results of the classical WENO scheme with MGFM; squares: the results of the modified HWENO scheme with MGFM; triangles: the results of the WENO-Z scheme with MGFM. Grid points: 200.

where Inflow/outflow boundary conditions are applied here. The final time t is 0.0007. We present the computed density ρ, velocity μ and pressure p by the classical WENO, WENO-Z and modified HWENO schemes with MGFM against the exact solution in Fig. 3, which illustrates the three schemes capture the location of the material interface correctly and simulate this problem well, meanwhile, to show the good performance of the HWENO scheme, we also give their partial enlarged pictures in the bottom of Fig. 3, and we can see the HWENO scheme has higher resolution than WENO schemes with slightly less transition points across the shock as the HWENO scheme is more compact than the WENO schemes. In addition, the HWENO scheme only needs to define the ghost fluid status at 2 points for other mediums, while the ghost fluid status at 3 points has to be defined for the WENO schemes. For saving space, we only give the partial enlarged picture in this problem, while for other problems, the HWENO scheme has less transition points across the shock too, and we also can see it from the modified HWENO scheme [51] for the single-medium flow problems.

Example 3.2. This problem contains a right going shock refracting at an air-helium interface with a reflected rarefaction wave, which is also taken from [8], and the initial

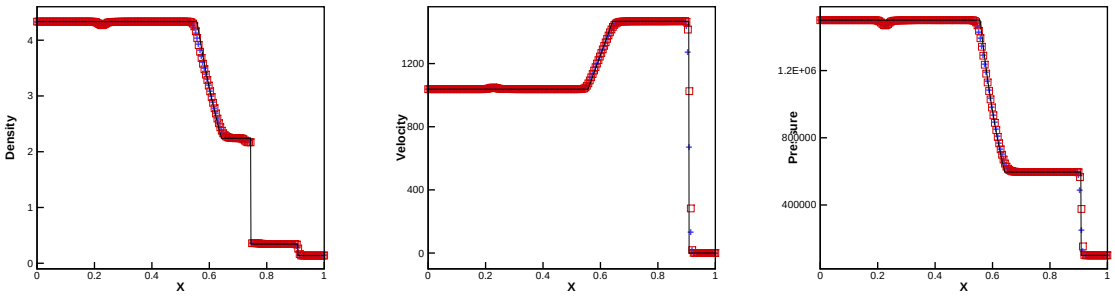

Figure 4: Example 3.2. $t=0.0005$. From left to right: density; velocity; pressure. Solid line: the exact solution; plus signs: the results of the classical WENO scheme with MGFM; squares: the results of the modified HWENO scheme with MGFM. Grid points: 200.

conditions are

$$(\rho,\mu,p,\gamma)=\begin{cases}(4.3333,3.2817\sqrt{10^5},1.5\times10^6,1.4), & x\in[0,0.05),\\ (1,0,1\times10^5,1.4), & x\in[0.05,0.5),\\ (0.1379,0,1\times10^5,5/3), & x\in[0.5,1],\end{cases}$$

with inflow and outflow boundary conditions. The location of the interface between air and helium is $x=0.5$, and the initial strength of the shock is $p_l/p_R=15$ at $x=0.05$. The final time is 0.0005, and we show the computed density ρ, velocity μ and pressure p by the classical WENO and modified HWENO schemes with MGFM against the exact solution in Fig. 4, then, we first can see that the contact discontinuity between two gases is located in the correct cell, and two schemes have similar results.

Example 3.3. We solve the one-dimensional Euler equations (2.1) with the following Riemann initial conditions as

$$(\rho,\mu,p,\gamma)=\begin{cases}(1.3333,0.3535\sqrt{10^5},1.5\times10^5,1.4), & x\in[0,0.05),\\ (1,0,1\times10^5,1.4), & x\in[0.05,0.5),\\ (3.1538,0,1\times10^5,1.249), & x\in[0.5,1].\end{cases}$$

The final time t is up to 0.0017. This example is taken from [8] too. We present the computed density ρ, velocity μ and pressure p by the classical WENO and modified HWENO schemes combined with MGFM against the exact solution in Fig. 5, and we can see the two schemes capture the correct location of the interface, with non-oscillations and similar comparable results.

Example 3.4. This problem has a strong shock on a gas-gas interface, and it is taken from [25]. The strength of the right shock wave is up to $p_L/p_R=100$, and the initial

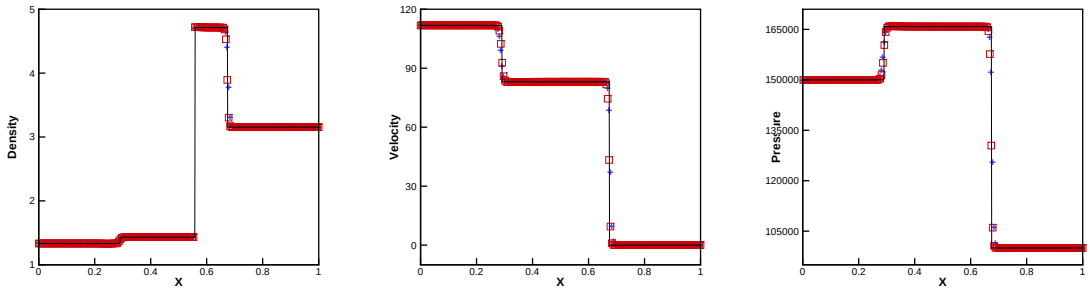

Figure 5: Example 3.3. $t=0.0017$. From left to right: density; velocity; pressure. Solid line: the exact solution; plus signs: the results of the classical WENO scheme with MGFM; squares: the results of the modified HWENO scheme with MGFM. Grid points: 200.

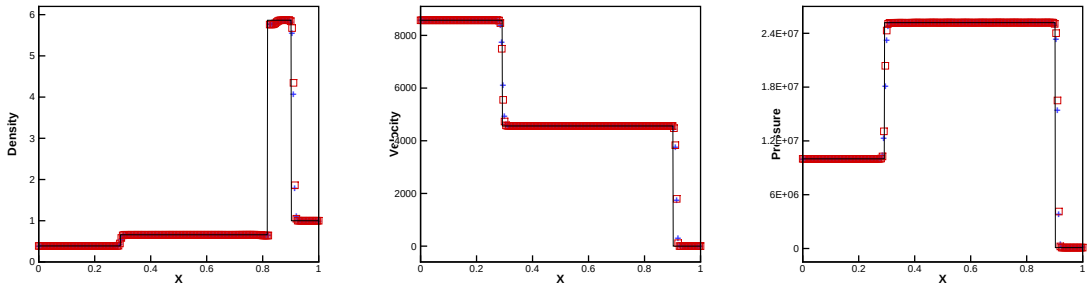

Figure 6: Example 3.4. $t=0.0001$. From left to right: density; velocity; pressure. Solid line: the exact solution; plus signs: the results of the classical WENO scheme with MGFM; squares: the results of the modified HWENO scheme with MGFM. Grid points: 200.

conditions are

$$(\rho,\mu,p,\gamma)=\begin{cases}(0.3884,27.1123\sqrt{10^5},1.0\times10^7,5/3), & x\in[0,0.3),\\ (0.1,0,1\times10^5,5/3), & x\in[0.3,0.4),\\ (1,0,1\times10^5,1.4), & x\in[0.4,1].\end{cases}$$

At the final time 0.0001, the computed density ρ, velocity μ and pressure p by the classical WENO and modified HWENO schemes combined with MGFM against the exact solution are given in Fig. 6, which illustrates that the two schemes work well for this gas-gas interaction problem, and they capture the correct location of the material interface.

Example 3.5. Now, we solve a gas-water shock tube problem taken from [32] with the following initial conditions as

$$(\rho,\mu,p,\gamma)^T=\begin{cases}(1270,0,8\times10^8,1.4)^T, & x\in[0,0.5),\\ (1000,0,1\times10^5,7.15)^T, & x\in[0.5,1],\end{cases}$$

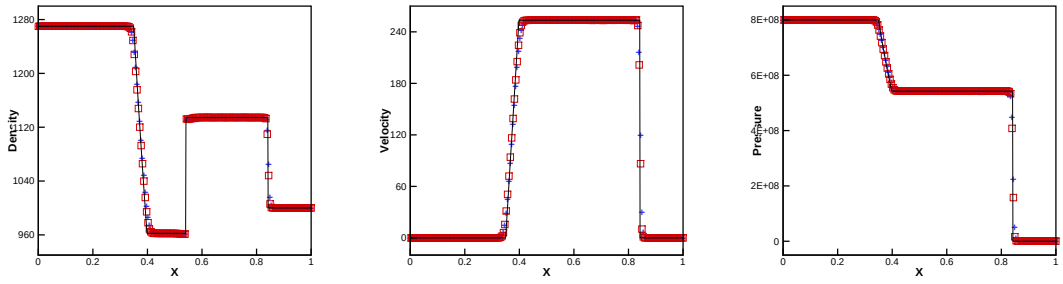

Figure 7: Example 3.5. $t=0.00016$. From left to right: density; velocity; pressure. Solid line: the exact solution; plus signs: the results of the classical WENO scheme with MGFM; squares: the results of the modified HWENO scheme with MGFM. Grid points: 200.

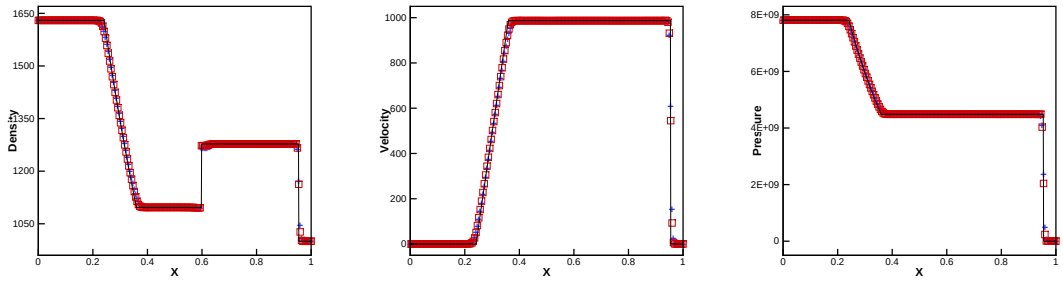

Figure 8: Example 3.6. $t=0.0001$. From left to right: density; velocity; pressure. Solid line: the exact solution; plus signs: the results of the classical WENO scheme with MGFM; squares: the results of the modified HWENO scheme with MGFM. Grid points: 200.

then, we can see that this underwater explosion problem has extremely high pressure in the gas medium, which would leads to a quite strong shock wave in the water medium. The final time is up to 0.00016, and we give the computed density ρ, velocity μ and pressure p by the classical WENO and modified HWENO schemes combined with MGFM against the exact solution in Fig. 7, which shows two schemes work well and capture the correct location of the material interface.

Example 3.6. This gas-water shock tube problem has higher energy of the explosive gaseous medium than the initial conditions in Example 3.5, and it is also taken from [32]. The initial conditions are given as

$$(\rho,\mu,p,\gamma)^T=\begin{cases}(1630,0,7.81\times10^9,1.4)^T, & x\in[0,0.5),\\ (1000,0,1\times10^5,7.15)^T, & x\in[0.5,1].\end{cases}$$

The final time is 0.0001, then, the computed density ρ, velocity μ and pressure p by the classical WENO and modified HWENO schemes combined with MGFM against the exact solution are presented in Fig. 8, then, we can know two schemes work well for this tough

gas-water problem with non-oscillations in the discontinuous regions, and the material interface between two mediums is also captured rightly.

Example 3.7. Now, we solve the governing equations (2.1) for two-dimensional Euler equations, and we first consider a problem with a Mach 1.22 air shock acting on a helium bubble, and we show its physical initial schematic picture in the left of Fig. 9. For the top and bottom boundaries, the reflective conditions are applied here, while the inflow and outflow conditions are given in the left and right boundaries, respectively. The non-dimensionalized initial conditions are

$$(\rho,\mu,\nu,p,\gamma)=\begin{cases}(1,0,0,1,1.4), & \text{pre-shocked air},\\ (1.3764,0.394,0,1.5698,1.4), & \text{post-shocked air},\\ (0.138,0,0,5/3), & \text{helium},\end{cases}$$

$$\phi=\sqrt{x^2+y^2}-1, \quad \text{level set},$$

where the regions of $\phi\leq 0$ represents the helium and the regions of $\phi>0$ represents the air, meanwhile, the regions of $x<1.2$ are the post-shocked air state, then, we give the computed results for density at final time 0.5, 1.0, 2.0 and 4.0 with 560×480 uniform grid points in Fig. 10, and this problem also had been experimentally studied in [10], which also shows the numerical results are comparable to the experimental results. We stop the computational time at $t=4.0$ before the generation of the strong re-entrant jet, which is a complex physical phenomenon, and it might need to use quite fine meshes or adaptive refinement techniques introduced in [15,35].

Next, we would briefly describe the numerical results. Initially, a shock hits the helium bubble, then, the incident shock partly refracts into the helium bubble, and other part of the incident shock reflects from the surface and returns the air. At $t=0.5$, since the sound speed in helium is faster than that in air, the initial regular shock becomes irregular and has the bifurcation of the shock on the bubble surface, and the experimental results

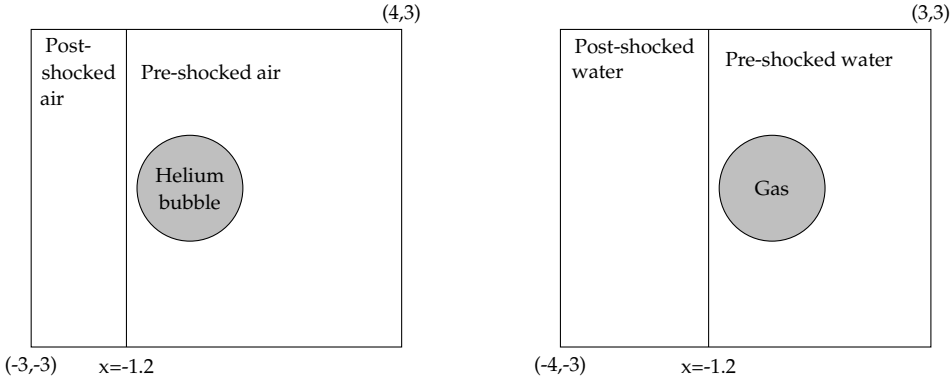

Figure 9: Physical domain for Example 3.7 (left) and Example 3.8 (right).

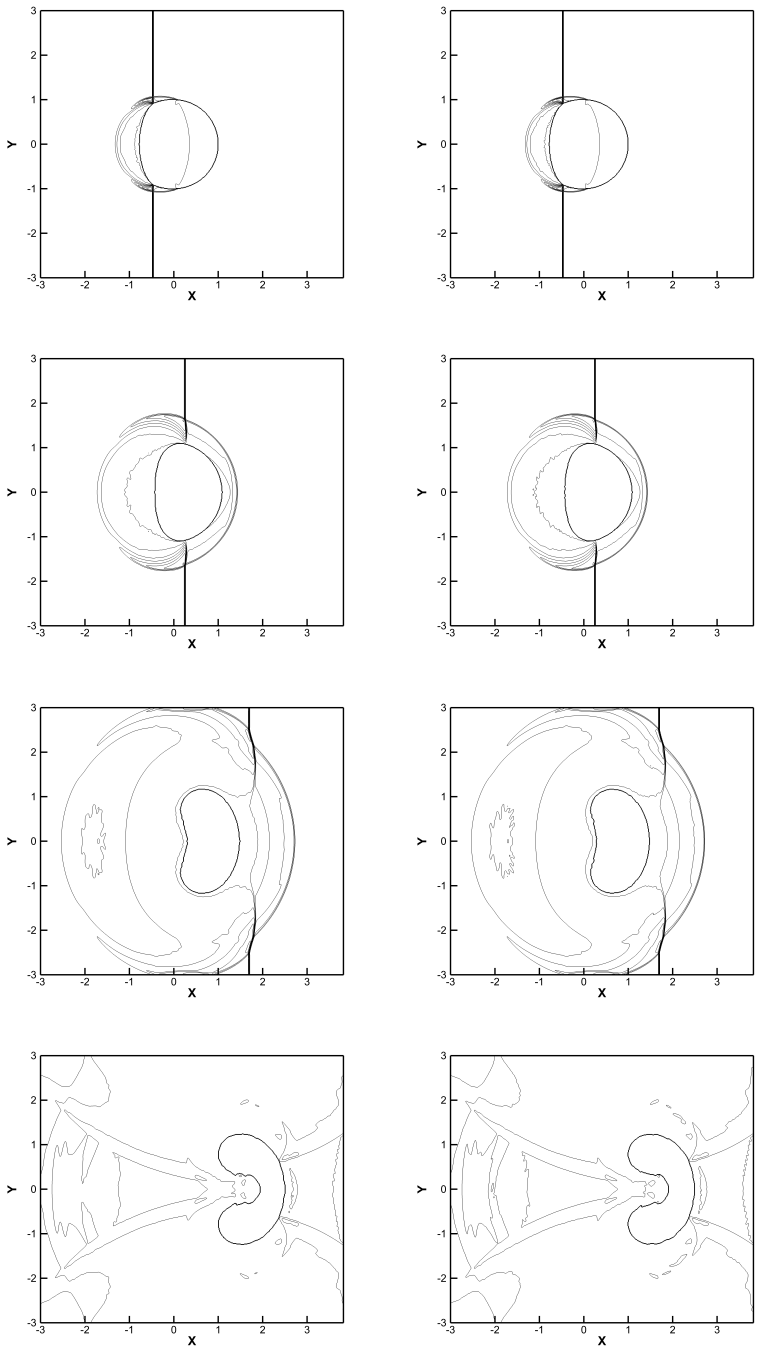

Figure 10: Example 3.7. The results computed by the classical WENO scheme (left) and modified HWENO scheme (right) with MGFM. 30 equally spaced density contours from 0.1 to 1.6. From top to bottom are $t=0.5$, $t=1.0$, $t=2.0$ and $t=4.0$, respectively. Grid points: 560×480.

given in [10] also illustrated it. At $t=1.0$, the refracted shock inside the helium bubble has interacted with the tail of the bubble and transmits into the air, when the incident shock just went through the top of the bubble. Later, the whole helium bubble starts to move to the right. At $t=2.0$, the incident shock has passed over the whole bubble, then, the shape of the bubble becomes deformed. Since then, a re-entrant jet begins to generate. Finally, the re-entrant jet has been formed at time $t=4.0$, which would leads to the instability of the interface. As time passes, the re-entrant jet becomes stronger and stronger, which would impact on the rear side of the bubble and make the bubble become collapse, and in this case, the quite fine meshes or adaptive refinement techniques [15, 35] might be needed.

Example 3.8. The final 2D example is a Mach 1.653 planar underwater shock interacting with a gas bubble, which is taken from [32], then, we solve the two-dimensional Euler equations (2.1) with the following non-dimensionalized initial conditions as

$$(\rho,\mu,\nu,p,\gamma)=\begin{cases}(1000,0,0,1,7.15), & \text{pre-shocked water},\\ (1176.3333,1.1692,0,9120,7.15), & \text{post-shocked water},\\ (1,0,0,1.4), & \text{gas},\end{cases}$$

$$\phi=\sqrt{x^2+y^2}-1, \quad \text{level set},$$

in which $\phi\leq 0$ represents the regions of gas and $\phi>0$ represents the regions of water, and the regions of $x<1.2$ is the post-shocked water state. The physical initial schematic picture is shown in the right of Fig. 9. For the top and bottom boundaries, the reflective boundary conditions are applied, and for the left and right boundaries, the inflow and outflow boundary conditions are employed, respectively. We show the computed density by the classical WENO and modified HWENO schemes at several times $t=0.06$, $t=0.19$, $t=0.357$ and $=0.481$ with 560×480 uniform grid points, and we can see the numerical results are comparable with that given by the discontinuous Galerkin finite element methods with MGFM [32]. The detailed physical analysis can be seen in [24] for the earlier stage, while one can be found in [30] for the late time. Overall, the WENO and HWENO schemes have similar numerical results for this example, but the HWENO scheme is more compact than the WENO scheme, which makes us to deal with the relatively simple interface and boundary conditions.

4 Concluding remarks

In this paper, we combine the modified HWENO scheme [51] with the modified ghost fluid method [25] to simulate the compressible two-medium flow problems. Comparing with the classical fifth order finite difference WENO scheme [14], the HWENO scheme is more compact since only immediate neighbor information is used in the reconstructions which leads to higher resolutions near the discontinuities, even though they both

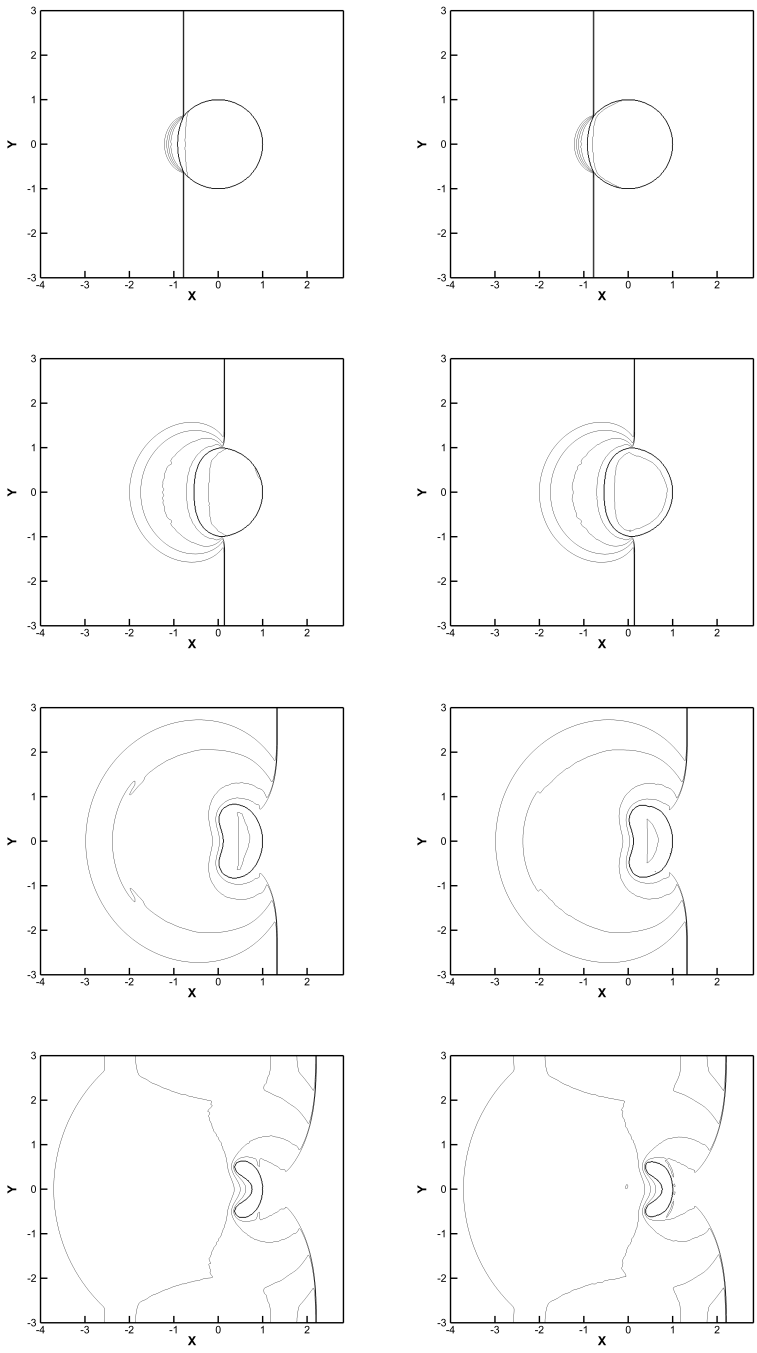

Figure 11: Example 3.8. The results computed by the classical WENO scheme (left) and modified HWENO scheme (right) with MGFM. 30 equally spaced density contours from 1.0 to 1200. From top to bottom are $t=0.06$, $t=0.19$, $t=0.357$ and $t=0.481$, respectively. Grid points: 560×480.

achieve the fifth order numerical accuracy. Furthermore, the HWENO scheme combined with the MGFM is very suitable for the simulation of the compressible two-medium flow problems because the HWENO scheme defines less ghost fluid information, which leads to a simpler method in dealing with the interface and boundary conditions. In addition, the HWENO method combined with the MGFM is very robust in simulating the gas-gas and gas-water interaction problems. The numerical results in this paper illustrate the good performances of the modified HWENO scheme with the modified ghost fluid method.

Acknowledgments

Z. Zhao and J. Qiu were supported partly by Science Challenge Project (China), No. TZ 2016002 and National Natural Science Foundation (China) grant 12071392. This work was carried out while Z. Zhao was visiting the Department of Applied and Computational Mathematics and Statistics, the University of Notre Dame under the support by the China Scholarship Council (CSC: 201906310075).

References

[1] R. Abgrall, How to prevent oscillations in multicomponent flow calculations: A quasi conservative approach, J. Comput. Phys., 125 (1996), 150-160.
[2] R. Abgrall and S. Karni, Computations of compressible multifluids, J. Comput. Phys., 169 (2001), 594-623.
[3] B. Biswas, R. Dubey, ENO and WENO schemes using arc-length based smoothness measurement, Comput. Math. Appl., 80(2020), 2780-2795.
[4] R. Borges, M. Carmona, B. Costaa and W.S. Don, An improved weighted essentially non-oscillatory scheme for hyperbolicconservation laws, J. Comput. Phys., 227 (2008), 3101-3211.
[5] X. Cai, X. Zhang and J. Qiu, Positivity-preserving high order finite volume HWENO schemes for compressible Euler equations, J. Sci. Comput., 68 (2016), 464-483.
[6] T.-J. Chen and C.H. Cooke, On the Riemann problem for liquid or gas-liquid media, Int. J. Numer. Meth. Fluid., 18 (1994), 529-541.
[7] Y. Chen and S. Jiang, A non-oscillatory kinetic scheme for multi-component flows with equation of state for a stiffened gas, J. Comput. Math., 29 (2011), 661-683.
[8] R.P. Fedkiw, T. Aslam, B. Merriman and S. Osher, A non-oscillatory Eulerian approach to interfaces in multimaterial flows (the ghost fluid method), J. Comput. Phys., 152 (1999), 457-492.
[9] J. Glimm, J.W. Grove, X.L. Li, K.-M. Shyue, Y. Zheng and Q. Zhang, Three-dimensional front tracking, SIAM J. Sci. Comput., 19 (1998), 703-727.
[10] J.-F. Haas and B. Sturtevant, Interaction of weak shock waves with cylindrical and spherical gas inhomogeneities, J. Fluid Mech., 181 (1987), 41-76.
[11] A. Harten, B. Engquist, S. Osher and S. Chakravarthy, Uniformly high order accurate essentially non-oscillatory schemes III, J. Comput. Phys., 71 (1987), 231-323.
[12] C. Hirt and B. Nichols, Volume of fluid (VOF) method for the dynamics of free boundaries, J. Comput. Phys., 39 (1981), 201-225.

[13] X.Y. Hu and B.C. Khoo, An interface interaction method for compressible multifluids, J. Comput. Phys., 198 (2004), 35-64.
[14] G.-S. Jiang and C.-W. Shu, Efficient implementation of weighted ENO schemes, J. Comput. Phys., 126 (1996), 202-228.
[15] E. Johnsen and T. Colonius, Implementation of WENO schemes in compressible multicomponent flow problems, J. Comput. Phys., 219 (2006), 715-732.
[16] S. Karni, Multicomponent flow calculations by a consistent primitive algorithm, J. Comput. Phys., 112 (1994), 31-43.
[17] B. Larrouturou, How to preserve the mass fractions positivity when computing compressible multicomponent flows, J. Comput. Phys., 95 (1991), 59-84.
[18] Y. Li, J. Cheng, Y. Xia and C.-W. Shu, High order arbitrary Lagrangian-Eulerian finite difference WENO scheme for Hamilton-Jacobi equations, Commun. Comput. Phys., 26 (2019), 1530-1574.
[19] T.G. Liu, C.L. Feng and L. Xu, Modified Ghost Fluid Method with Acceleration Correction (MGFM/AC), J. Sci. Comput., 81 (2019), 1906-1944.
[20] C. Liu and C. Hu, An adaptive high order WENO solver for conservation laws, Commun. Comput. Phys., 26 (2019), 719-748.
[21] T.G. Liu and B.C. Khoo, The accuracy of the modified ghost fluid method for gas-gas Riemann problem, Adv. Appl. Math., 57 (2007), 721-733.
[22] T.G. Liu, B.C. Khoo and W.F. Xie, The modified ghost fluid method as applied to extreme fluid-structure interaction in the presence of cavitation, Commun. Comput. Phys., 1 (2006), 898-919.
[23] T.G. Liu, B.C. Khoo and K.S. Yeo, The simulation of compressible multi-medium flow. Part I: A new methodology with applications to 1D gas-gas and gas-water cases, Comput. Fluid., 30 (2001), 291-314.
[24] T.G. Liu, B.C. Khoo and K.S. Yeo, The simulation of compressible multi-medium flow. Part II: Applications to 2D underwater shock refraction, Comput. Fluid., 30 (2001), 315-337.
[25] T.G. Liu, B.C. Khoo and K.S. Yeo, Ghost fluid method for strong shock impacting on material interface, J. Comput. Phys., 190 (2003), 651-681.
[26] X.D. Liu, S. Osher and T. Chan, Weighted essentially non-oscillatory schemes, J. Comput. Phys., 115 (1994), 200-212.
[27] H. Liu and J. Qiu, Finite difference Hermite WENO schemes for conservation laws, J. Sci. Comput., 63 (2015), 548-572.
[28] T.G. Liu, W.F. Xie and B.C. Khoo, The modified ghost fluid method for coupling of fluid and structure constituted with hydro-elasto-plastic equation of state, SIAM J. Sci. Comput., 30 (2008), 1105-1130.
[29] Z. Ma and S.P. Wu, HWENO schemes based on compact difference for hyperbolic conservation laws, J. Sci. Comput., 76 (2018), 1301-1325.
[30] R.R. Nourgaliev, T.N. Dinh and T.G. Theofanous, Adaptive characteristic-based matching for compressible multifluid dynamics, J. Comput. Phys., 213 (2006), 500-529.
[31] J. Qiu, T.G. Liu and B.C. Khoo, Runge-Kutta discontinuous Galerkin methods for compressible two-medium flow simulations: One-dimensional case, J. Comput. Phys., 222 (2007), 353-373.
[32] J. Qiu, T.G Liu and B.C. Khoo, Simulations of compressible two-medium flow by Runge-Kutta discontinuous Galerkin methods with the ghost fluid method, Commun. Comput. Phys., 3 (2008) 479-504.
[33] J. Qiu and C.-W. Shu, Hermite WENO schemes and their application as limiters for Runge-

Kutta discontinuous Galerkin method: one-dimensional case, J. Comput. Phys., 193 (2004), 115-135.
[34] J. Qiu and C.-W. Shu, Hermite WENO schemes and their application as limiters for Runge-Kutta discontinuous Galerkin method II: Two dimensional case, Comput. Fluid., 34 (2005), 642-663.
[35] J.J. Quirk and S. Karni, On the dynamics of a shock-bubble interaction, J. Fluid Mech., 318 (1996), 129-163.
[36] R. Saurel and R. Abgrall, A simple method for compressible multifluid flows, SIAM J. Sci. Comput., 21 (1999), 1115-1145.
[37] C.-W. Shu, Essentially non-oscillatory and weighted essentially non-oscillatory schemes, Acta Numerica, 29 (2020), 701-762.
[38] C.-W. Shu and S. Osher, Efficient implementation of essentially non-oscillatory shock capturing schemes, J. Comput. Phys., 77 (1988), 439-471.
[39] K.-M. Shyue, An efficient shock-capturing algorithm for compressible multicomponent problems, J. Comput. Phys., 142 (1998), 208-242.
[40] M. Sussman, P. Smereka and S. Osher, A level set approach for computing solutions to incompressible two-phase flow, J. Comput. Phys., 114 (1994), 146-159.
[41] Z. Tao, F. Li and J. Qiu, High-order central Hermite WENO schemes on staggered meshes for hyperbolic conservation laws, J. Comput. Phys., 281 (2015), 148-176.
[42] S.O. Unverdi and G. Tryggvason, A front-tracking method for viscous incompressible multi-fluid flows, J. Comput. Phys., 100 (1992), 25-37.
[43] C.W. Wang, T.G. Liu and B.C. Khoo, A real-ghost fluid method for the simulation of multi-medium compressible flow, SIAM J. Sci. Comput., 28 (2006), 278-302.
[44] L. Xu, C.L. Feng and T.G. Liu, Practical techniques in ghost fluid method for compressible multi-medium flows, Commun. Comput. Phys., 20 (2016), 619-659.
[45] L. Xu and T.G. Liu, Optimal error estimation of the modified ghost fluid method, Commun. Comput. Phys., 8 (2010), 403-426.
[46] L. Xu and T.G. Liu, Modified ghost fluid method as applied to fluid-plate interaction, Adv. Appl. Math. Mech., 6 (2014), 24-48.
[47] Y.H. Zahran and A.H. Abdalla, Seventh order Hermite WENO scheme for hyperbolic conservation laws, Comput. Fluid., 131 (2016), 66-80.
[48] Z. Zhao, Y. Chen and J. Qiu, A hybrid Hermite WENO scheme for hyperbolic conservation laws, J. Comput. Phys., 405 (2020), 109175.
[49] Z. Zhao, Y. Chen and J. Qiu, A hybrid WENO method with modified ghost fluid method for compressible two-medium flow problems, Numer. Math.: Theory, Methods and Appl., to appear, http://arxiv.org/abs/2009.00461.
[50] Z. Zhao and J. Qiu, A Hermite WENO scheme with artificial linear weights for hyperbolic conservation laws, J. Comput. Phys., 417 (2020), 109583.
[51] Z. Zhao, Y.-T. Zhang and J. Qiu, A modified fifth order finite difference Hermite WENO scheme for hyperbolic conservation laws, J. Sci. Comput., 85 (2020), 29.
[52] J. Zhu and J. Qiu, A class of fourth order finite volume Hermite weighted essentially non-oscillatory schemes, Sci. China Ser. A Math., 51 (2008), 1549-1560.